

Phase separation in tilings of a bounded region of the plane

Eduardo J. Aguilar,¹ Valmir C. Barbosa,^{2,*} Raul Donangelo,^{3,4} and Sergio R. Souza^{4,5,6}

¹*Instituto de Ciência e Tecnologia, Universidade Federal de Alfenas,
Rod. José Aurélio Vilela, 11999, 37715-400 Poços de Caldas - MG, Brazil*

²*Programa de Engenharia de Sistemas e Computação, COPPE,
Universidade Federal do Rio de Janeiro, Centro de Tecnologia,
Sala H-319, 21941-914 Rio de Janeiro - RJ, Brazil*

³*Instituto de Física, Facultad de Ingeniería, Universidad de la República,
Julio Herrera y Reissig 565, 11.300 Montevideo, Uruguay*

⁴*Instituto de Física, Universidade Federal do Rio de Janeiro,
Centro de Tecnologia, Bloco A, 21941-909 Rio de Janeiro - RJ, Brazil*

⁵*Departamento de Engenharia Nuclear, Universidade Federal de Minas Gerais,
Av. Antônio Carlos, 6627, 31270-901 Belo Horizonte - MG, Brazil*

⁶*Departamento de Física, ICEX, Universidade Federal Fluminense,
R. Desembargador Ellis Hermydio Figueira, Aterrado, 27213-145 Volta Redonda - RJ, Brazil*

Given a finite collection of two-dimensional tile types, the field of study concerned with covering the plane with tiles of these types exclusively has a long history, having enjoyed great prominence in the last six to seven decades, not only as a topic of recreational mathematics but mainly as a topic of great scientific interest. Much of this interest has revolved around fundamental geometrical problems such as minimizing the variety of tile types to be used, and also around important applications in areas such as crystallography as well as others concerned with various atomic- and molecular-scale phenomena. All these applications are of course confined to finite spatial regions, but in many cases they refer back directly to progress in tiling the whole, unbounded plane. Tilings of bounded regions of the plane have also been actively studied, but in general the additional complications imposed by the boundary conditions tend to constrain progress to mostly indirect results, such as recurrence relations, for example. Here we study the tiling of rectangular regions of the plane by rectangular tiles. The tile types we use are squares, dominoes, and straight tetraminoes. For this set of tile types, not even recurrence relations seem to be available. Our approach is to seek to characterize this system through some of the fundamental quantities of statistical physics. We do this on two parallel tracks, one fully analytical for what seems to be the most complex special case still amenable to such approach, the other based on the Wang-Landau method for state-density estimation. Given a simple Hamiltonian based solely on tile contacts, we have found either approach to lead to illuminating depictions of entropy, temperature, and above all phase separation. The notion of phase separation, in this context, refers to keeping track of how many tiles of each type are used in each of the many possibilities. We have found that this helps bind together different aspects of the system in question and conjecture that future applications will benefit from the possibilities it affords.

I. INTRODUCTION

A tiling of the plane, given a finite collection C of tile types, is a covering that allows for no superposition of tiles and no gaps between them while employing tiles of types in C and no others. Depending on the tile types that constitute it, C is said to be periodic, non-periodic, or aperiodic. It is periodic if its tile types only admit patterns that repeat themselves indefinitely, which is the case, for example, of the regular hexagon as the only tile type in C . If C admits not only such repetitiveness but also indefinite pattern diversification, for example when it only comprises the equilateral triangle or the square, then it is called non-periodic. C is called aperiodic when indefinite diversification is the only possibility.

The first aperiodic tile set to be discovered dates from 1966 [1] and uses over twenty thousand types of the edge-colored square tiles known as Wang tiles. Tiling the plane

with Wang tiles had been devised in the context of studying the decidability of decision problems [2], and as such required tiling rules beyond the prohibition of superpositions or gaps. The resulting aperiodicity quickly sparked an interest for finding smaller tile-type sets, which within a few years led to the discovery of an aperiodic set with only six types [3]. The well-known Penrose aperiodic sets were then soon discovered [4–6], first with six edge-marked types (three varieties of the regular pentagon and three other shapes to fill gaps, thereby completing work that Kepler had undertaken in the early 17th century), then with either one dart and one kite, as the tiles became known, or two rhombi. The first aperiodic monotile (a so-called “einstein,” a single tile type with which the plane can be tiled without ever incurring periodicity) was discovered only very recently [7]. This monotile is one of the 873 eight-kite polykites [8] and has been named the hat. Notably, a polykite’s basis kite is not the same as the Penrose kite. The discovery of the hat was soon followed by that of specters, monotiles closely related to the

* valmir@cos.ufrj.br

hat but having the property of being chiral, i.e., of tiling the plane without ever being reflected [9].

The two-rhombus Penrose tile set, both as proposed and in a generalization to three dimensions, has had enduring impact in important fields, particularly in crystallography, where the patterns it generates were found to suggest structural ordering outside the classical approach (see [10] and references therein). This connection foreshadowed the discovery of quasicrystals that soon followed [11] and has since continued to influence the field [12]. Other applications of the Penrose tile sets include modeling jammed solids [13] and the study of graph-theoretic properties of the classical dimer model [14]. Beyond the direct applicability of specific aperiodic tile sets, the very notion of their aperiodicity has had far-reaching influence, e.g., in interpreting the results of self-assembled crystal structures from molecular building blocks [15] and in demonstrating the use of “algorithmic” self-assembly of DNA strands into cellular automata (specifically, one based on Wolfram’s elementary rule 90, the XOR rule [16]; see [17] and references therein). In fact, self-assembled systems are now part of cutting-edge research in various fields, as in materials science [18] and DNA-based computing [19–22].

Of course, all these applications that ultimately refer back to tilings of the plane are actually confined to finite regions, where the periodicity of the tile-type collection C ceases to have meaning, as do the issues regarding decidability that helped spark the whole field decades ago. Instead, given finiteness, the focus shifts to counting the tilings that C admits, with worries concerning undecidability giving way to the concrete possibility of computational intractability. In fact, even though finding tilings of a finite region of the plane can be achieved by solving a binary integer programming problem [23], in general this problem is computationally intractable in the sense of NP-hardness [24, 25].

Here we consider the tiling of rectangular regions when C contains rectangles exclusively. We study some of the statistical physics of the remarkably complex system that results, even for a close to minimal C , as the great variety of possible tilings is taken into account. Using a Hamiltonian that depends only on inter-tile contact, we study entropy, temperature, and most importantly phase separation. In the context of tiling a finite region of the plain, focusing on how many tiles of each type in C is used provides a means to highlight specific interactions between tile structure, energy, and entropy. We do succeed in describing a special case fully analytically, but in the general case we resort to the Wang-Landau method to estimate state density [26, 27], with states now understood as tilings, before analysis can be carried out.

We proceed as follows. We briefly review the current knowledge of tiling rectangles by rectangles in Sec. II, where we also introduce the C and Hamiltonian we use. In Sec. III we analyze the special case we mentioned and in Sec. IV we tackle the general case. We conclude in Sec. V.

II. TILINGS OF A RECTANGULAR BOARD WITH RECTANGLES

In order to study the statistical physics of tilings with rectangular tiles of an $m \times n$ rectangular board (a board with mn 1×1 cells), the central entity to be considered is the number k_{mn} of possible distinct tilings. Obtaining a closed-form expression for k_{mn} depends not only on the values of m and n but also on which tile types are to be used. Notably, already for arbitrary $m, n \geq 2$ it seems that such an expression is known only for the case in which dominoes (1×2 or 2×1 tiles) are the only tiles used. In this case, each tiling requires $mn/2$ dominoes and k_{mn} is given by the surprising formula

$$k_{mn} = \prod_{i=1}^{\lceil \frac{m}{2} \rceil} \prod_{j=1}^{\lceil \frac{n}{2} \rceil} \left(4 \cos^2 \frac{\pi i}{m+1} + 4 \cos^2 \frac{\pi j}{n+1} \right), \quad (1)$$

which as required is nonzero if and only if mn is even [28, 29].¹ If more tile types are to be used, then recurrence relations and generating functions can still be obtained, but only in a limited manner. In fact, fixing $m = 2$ and leaving n unconstrained while squares (1×1 tiles) and dominoes are the allowed tile types seems to be as far as one can go (see, e.g., [30]).

In this study we consider tilings with squares, dominoes and straight tetraminoes (1×4 or 4×1 tiles, henceforth simply tetraminoes) exclusively, though methodologically it is in principle possible to generalize to a greater variety of tile types. We denote by n_1 the number of squares to be used in a tiling, by n_2 the number of dominoes, and by n_4 the number of tetraminoes. A joint assignment of values to n_1, n_2, n_4 admits at least one tiling of the board if and only if $mn = n_1 + 2n_2 + 4n_4$. We refer to such an assignment as a configuration of the system.

Given a configuration of the system, and considering any tiling it admits, let u and v be any two of the tiles used. We denote by $[u|v]$ the tile-perimeter length that is common to u and v . It follows that $[u|v] > 0$ if and only if u and v are adjacent to each other in the tiling in question. Additionally, the sum of $[u|v]$ over all u, v pairs is conserved over all possible tilings for the same configuration, since in any such tiling every tile contributes half its perimeter to the sum, discounting those tile edges that coincide with the board’s own perimeter and therefore contribute nothing. This sum quantifies all inter-tile contacts and is here used as the system’s Hamiltonian. That is,

$$H(n_1, n_2) = \sum_{\substack{u, v \in I(n_1, n_2) \\ u \neq v}} [u|v] \quad (2)$$

$$= 2n_1 + 3n_2 + 5n_4 - m - n, \quad (3)$$

¹ If both m and n are odd, then $\lceil m/2 \rceil = (m+1)/2$ and $\lceil n/2 \rceil = (n+1)/2$, which leads to a zero factor.

where I is the set comprising distinguishable versions of all $n_1 + n_2 + n_4$ tiles (so that I is in fact a set). In the above expression we write both H and I as functions of only n_1 and n_2 to highlight the simple fact that, given m and n , one of n_1, n_2, n_4 is necessarily a function of the other two. We have chosen n_4 for this role, so its value is to be determined as

$$n_4 = \frac{mn - n_1 - 2n_2}{4}. \quad (4)$$

It is often possible for energy levels h to exist such that $H(n_1, n_2) = h$ for more than one configuration of the system. For the purpose of discussing entropy and temperature, we handle such “degeneracy” both by focusing on each of the configurations involved independently of the others and by taking them into account together. Doing this allows for distinct perspectives from which to analyze the system.

III. A SPECIAL CASE

The most complex systems for which analytical treatment is possible in this three tile-type scenario seem to be those for which $m = 1$, that is, those whose board is $1 \times n$. In this case, we have

$$n_4 = \frac{n - n_1 - 2n_2}{4} \quad (5)$$

and

$$H(n_1, n_2) = n_1 + n_2 + n_4 - 1. \quad (6)$$

Moreover, given a configuration, the number of tilings it admits, now expressed as a function of only n_1, n_2 as well, is

$$k_{1n}(n_1, n_2) = (n_1, n_2, n_4)! = \frac{(n_1 + n_2 + n_4)!}{n_1! n_2! n_4!}, \quad (7)$$

which is the multinomial coefficient for n_1, n_2, n_4 . To continue, we first rewrite k_{1n} as

$$k_{1n}(n_1, n_2) = \frac{\Gamma(n_1 + n_2 + n_4 + 1)}{\Gamma(n_1 + 1) \Gamma(n_2 + 1) \Gamma(n_4 + 1)} \quad (8)$$

and whenever needed substitute the reals x, y for the integers n_1, n_2 , respectively, so that differentiation can be carried out properly. We also note that

$$\frac{\partial}{\partial w} \ln \Gamma(w) = \frac{\Gamma'(w)}{\Gamma(w)} = \psi_0(w), \quad (9)$$

where ψ_0 is the digamma function.

For $k > 0$ an integer, we have $\psi_0(k) = -\gamma$ if $k = 1$, $\psi_0(k) = \sum_{\ell=1}^{k-1} \ell^{-1} - \gamma$ if $k > 1$, where $\gamma \approx 0.5772$ is the Euler constant. It follows, e.g., that $\Gamma'(w) \approx 0.4228, 1.8456, 7.5366, 36.1464$ for $w = 2, 3, 4, 5$, while an

approximation of what could pass for the “derivative” of the factorial function at the integer $w - 1$, given by

$$\frac{\Delta \Gamma(w)}{2} = \frac{\Gamma(w+1) - \Gamma(w-1)}{2}, \quad (10)$$

yields $2^{-1} \Delta \Gamma(w) = 0.5, 2.5, 11, 57$ for the same values of w . In addition, $\Gamma'(1)$ is unique in that it is negative. Thus, even though we do in the sequel use $\Gamma'(w)$ as a measure of the local variability of the factorial function at $w - 1$, some inconsistency is to be expected. We return to this in our analysis in Sec. III B.

For later reference, we note further that, by Eq. (6) and letting $a = n \bmod 4$, the possible values of H range from a minimum that uses as many tetraminoes as possible ($n_4 = \lfloor n/4 \rfloor$), and also as few dominoes ($n_2 = \lfloor a/2 \rfloor$) and squares ($n_1 = a \bmod 2$) as possible, to a maximum that only uses squares ($n_1 = n, n_2 = n_4 = 0$). This yields

$$H_{\min}^{1 \times n} = a \bmod 2 + \lfloor a/2 \rfloor + \lfloor n/4 \rfloor - 1 \quad (11)$$

$$= \lceil a/2 \rceil + \lfloor n/4 \rfloor - 1 \quad (12)$$

and

$$H_{\max}^{1 \times n} = n - 1. \quad (13)$$

A. The nondegenerate case

Analyzing the system from a configuration-centric perspective (i.e., by essentially ignoring the possible degeneracy of certain energy levels) amounts to regarding both entropy and temperature as functions of n_1, n_2 . That is,

$$S_{\text{nd}}(n_1, n_2) = \ln k_{1n}(n_1, n_2) \quad (14)$$

and, using Eq. (8) with $\Gamma'(w) = \Gamma(w)\psi_0(w)$,

$$T_{\text{nd}}^{-1}(n_1, n_2) = \left(\frac{\partial S_{\text{nd}}}{\partial x} \frac{\partial x}{\partial H} + \frac{\partial S_{\text{nd}}}{\partial y} \frac{\partial y}{\partial H} \right) \bigg|_{\substack{x=n_1 \\ y=n_2}} \quad (15)$$

$$= U(n_1, n_2), \quad (16)$$

where

$$U(n_1, n_2) = 2\psi_0(n_1 + n_2 + n_4 + 1) - \quad (17)$$

$$\frac{4}{3} \psi_0(n_1 + 1) - 2\psi_0(n_2 + 1) + \frac{4}{3} \psi_0(n_4 + 1).$$

Phase separation can be achieved in this case by fixing the value of, say, n_1 and observing the configurations that result as n_2 and n_4 are varied. Taking $n = 256$, for example, results in the 4225 configurations shown as background dots in the $H \times S_{\text{nd}}$ plots of Fig. 1. Each of panels A, B, C in the figure shows some of the phases that result from assigning fixed values to n_1, n_2, n_4 , respectively.

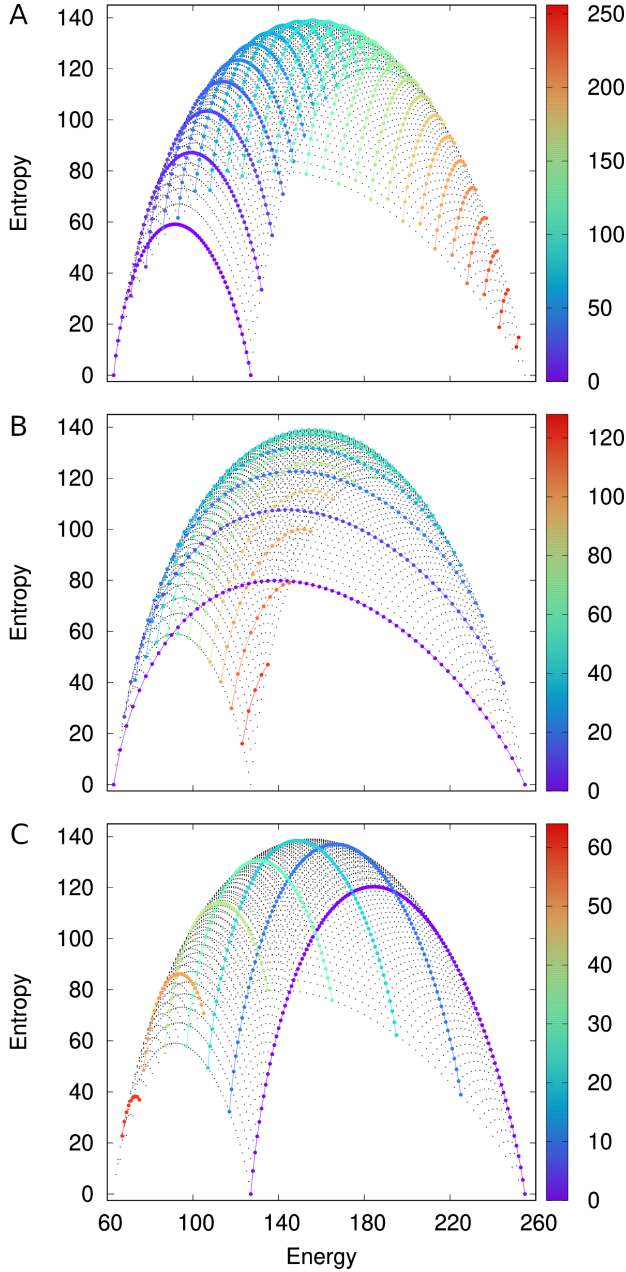


FIG. 1. Phase separation for $m = 1$, $n = 256$, shown against a backdrop of tiny black dots representing the 4225 configurations by their energy H and entropy S_{nd} . Phases are shown as larger, color-coded dots for selected (multiple-of-10) values of n_1 (A), n_2 (B), and n_4 (C). $H_{\min}^{1 \times 256} = 63$, $H_{\max}^{1 \times 256} = 255$.

B. The degenerate case

An alternative analysis strategy is to recognize the existence of degenerate energy levels and take it fully into account. For each value h in the interval from $H_{\min}^{1 \times n}$ to $H_{\max}^{1 \times n}$, the system's entropy and temperature are functions of h . Entropy is given by

$$S_d(h) = \ln K(h), \quad (18)$$

where

$$K(h) = \sum_{\substack{n_1, n_2 \\ H(n_1, n_2) = h}} k_{1n}(n_1, n_2), \quad (19)$$

and temperature is such that

$$T_d^{-1}(h) = \frac{\partial S_d}{\partial x} \frac{\partial x}{\partial H} + \frac{\partial S_d}{\partial y} \frac{\partial y}{\partial H} \quad (20)$$

$$= \frac{1}{K(h)} \sum_{\substack{n_1, n_2 \\ H(n_1, n_2) = h}} \left(\frac{\partial k_{1n}}{\partial x} \frac{\partial x}{\partial H} + \frac{\partial k_{1n}}{\partial y} \frac{\partial y}{\partial H} \right) \Big|_{\substack{x=n_1 \\ y=n_2}} \quad (21)$$

$$= \sum_{\substack{n_1, n_2 \\ H(n_1, n_2) = h}} \frac{k_{1n}(n_1, n_2)}{K(h)} U(n_1, n_2). \quad (22)$$

That is, $T_d^{-1}(h)$ is a convex combination of $U(n_1, n_2)$ for those configurations for which $H(n_1, n_2) = h$.

Thus, as far as representing configurations by their H and S_d values is concerned, all configurations for which the value of H is the same become conjoined in an $H \times S_d$ plot. This is illustrated in the panels of Fig. 2 for $n = 256$. As expected, this figure's panel A reveals a greater variety of configurations contributing to S_d near the midrange values of H . As for panel B, overall we also see T_d behave as expected, that is, slightly above zero and increasing before S_d peaks as H grows, then abruptly negative and increasing toward slightly below zero. However, a closer examination reveals a sudden flip back to positive temperatures for the highest four values of H : for $H = 252$ and only one of the two contributing configurations ($n_1 = 252, n_2 = 0, n_4 = 1$); for $H = 253$ and the only contributing configuration ($n_1 = 252, n_2 = 2, n_4 = 0$); for $H = 254$ and the only contributing configuration ($n_1 = 254, n_2 = 1, n_4 = 0$); and for $H = 255$ and the only contributing configuration ($n_1 = 256, n_2 = n_4 = 0$).

This can be further explored as in Fig. 3, which illustrates the behavior of T_d^{-1} according to both Eq. (22) and

$$T_d^{-1}(h) \approx \frac{S_d(h+1) - S_d(h-1)}{2}. \quad (23)$$

The sudden turn to positive temperatures described above is clearly visible, as is the overall discrepancy between the two curves. We attribute these differences to the problems that are inherent to using Γ' to assess the local variability of the factorial function, as discussed in the introduction to Sec. III. In spite of these difficulties, for most of the energy spectrum Eq. (22) provides a reasonable representation of the actual quantity. It is also significant that the use of Γ' is the only available analytical technique for temperature assessment in the case at hand.

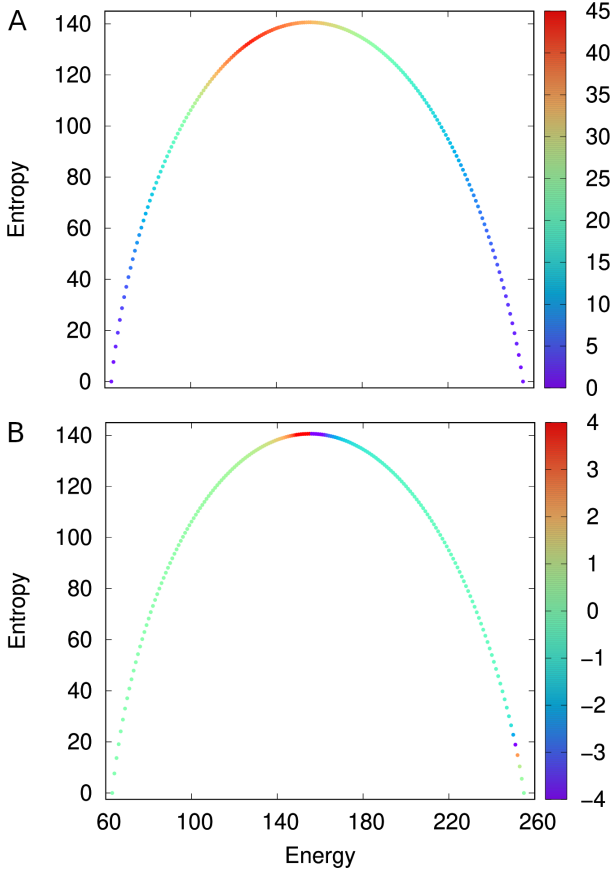


FIG. 2. Entropy S_d as a function of energy H for $m = 1$, $n = 256$. Dots are color-coded to indicate the number of configurations (A) and the temperature T_d (B) for each energy level. For readability, the color bar in (B) leaves out 7 points for which $T_d < -4$ and 6 others for which $T_d > 4$. These points get colored with the color corresponding to -4 or to 4 , respectively. $H_{\min}^{1 \times 256} = 63$, $H_{\max}^{1 \times 256} = 255$.

C. Remarks on computational tractability

In terms of the computational difficulties involved, an important point to note if we were to move beyond $n = 256$ is that obtaining plots like the ones in Figs. 1 and 2 would become increasingly harder. This is so because those plots contemplate all possible configurations of the system, which for $n = 1, 2, \dots, 2^{15}$ grows from 1 to 67 125 249, as shown in Fig. 4. These numbers are not particularly impressive, but already for $n = 2^{16}$ we found that 128 GB of memory were insufficient for the Mathematica 13 system to generate all configurations. (Regarding notation, in the caption of Fig. 4, and henceforth, we use the Iverson bracket $[P]$ for P a logical proposition. $[P]$ equals 1 if P is true, 0 if P is false. This notation generalizes the Kronecker delta, since $[i = j] = \delta_{ij}$.)

On the other hand, it must be kept in mind that Figs. 1 and 2 could only be obtained due to the availability of the closed-form expression for k_{1n} given in Eq. (8), which essentially does away with the need to count the number of

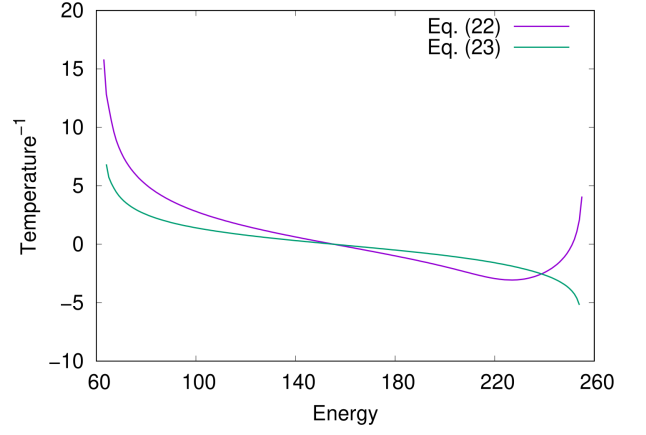


FIG. 3. T_d^{-1} as a function of energy H according to Eqs. (22) and (23).

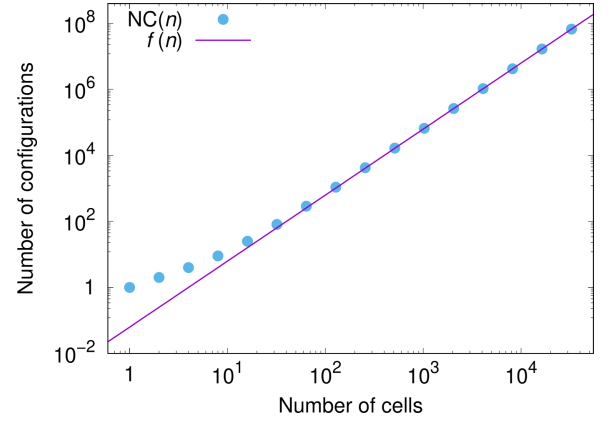


FIG. 4. Total number of configurations, for $m = 1$, as the function $NC(n)$ of the number of cells n . The power law that fits the points asymptotically is $f(n) = 4^{-2}n^2$. This comes from $NC(n) = \sum_{n_1=0}^n \sum_{n_2=0}^{\lfloor (n-n_1)/2 \rfloor} [(n - n_1 - 2n_2) \bmod 4 = 0] \approx \sum_{n_1=0}^n \sum_{n_2=0}^{\lfloor (n-n_1)/2 \rfloor} 4^{-1}$, which equals $4^{-2}(n+1)(n+3)$ if n is odd, $4^{-2}(n+2)^2$ if n is even. Either of these expressions tends asymptotically to $f(n)$. Counting each configuration as only 4^{-1} targets the many situations where the condition $(n - n_1 - 2n_2) \bmod 4 = 0$ fails, causing three out of four configurations to be invalid.

tilings admitted by each of the configurations in order to calculate entropy. Totalling this number over all configurations results in $\sum_h K(h)$, whose growth as a function of n is depicted in Fig. 5. Crucially, for $n = 256$ the value of $\sum_h K(h)$ is already of the order of 10^{63} , which can be expected to be surpassed by many orders of magnitude as we consider the $m > 1$ cases even for boards with a similar number of cells. Nothing like Eq. (8) is known for $m > 1$, so clearly generalizing the special case of $m = 1$ requires the ability to estimate entropy without counting the number of tilings admitted by any given configuration.

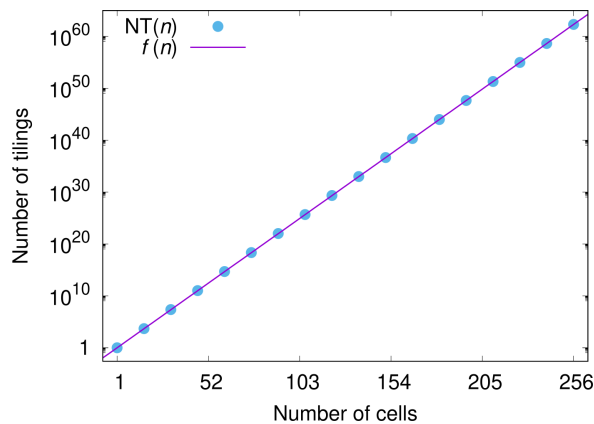


FIG. 5. Total number of tilings, for $m = 1$, as the function $\text{NT}(n) = \sum_h K(h)$ of the number of cells n . The exponential fitting the points is $f(n) = e^{0.562663(n-1)}$.

IV. THE GENERAL CASE

For the general case we follow the same two strategies used in Sec. III, i.e., we study both the nondegenerate case (by focusing on individual configurations even though in general there can be several of them for the same energy level) and the degenerate one. As previously, therefore, the first strategy essentially sidelines the issue of energy-level degeneracy, thus allowing phase separation to be highlighted as in Fig. 1. Our approach relies on sampling tilings randomly, calculating the energy level for each sample, then adding some contribution to the ongoing entropy estimate for that energy level.

A. Entropy estimation

Our approach to obtain entropy estimates is to use the Wang-Landau method [26, 27], which is a Monte Carlo Markov Chain (MCMC) method with well-established convergence properties [31, 32] to estimate state densities in statistical models. MCMC methods work by placing a walker at some randomly chosen initial state and then having it hop from state to state according to the chain's transition probabilities, recording information along the way until some stopping criterion is met. The specific formulation we use is derived from the Metropolis-Hastings method [33, 34], in which the transition probabilities are based on the chain's detailed-balance conditions and therefore make the desired stationary distribution explicit. Upon convergence to all detailed-balance conditions being satisfied, that is the distribution that will be observed (see Section IV B).

Given the values of m and n , the state space in this study is the set of all tilings of the $m \times n$ board by squares, dominoes, and tetraminoes. Each tiling is relative to a configuration unequivocally specified by the values of n_1 and n_2 . A tiling's target probability in the desired stationary distribution is proportional to $k_{mn}^{-1}(n_1, n_2)$, whose

value is unknown but can be estimated, once an estimate $\hat{S}(n_1, n_2)$ is available for the corresponding configuration's entropy $S(n_1, n_2)$, as $e^{-\hat{S}(n_1, n_2)}$. Thus, given two tilings t and $t' \neq t$, of configurations n_1, n_2 and n'_1, n'_2 , respectively, the detailed-balance condition for them reads

$$e^{-\hat{S}(n_1, n_2)} g_{t \rightarrow t'} a_{t \rightarrow t'} = e^{-\hat{S}(n'_1, n'_2)} g_{t' \rightarrow t} a_{t' \rightarrow t}, \quad (24)$$

where $g_{t \rightarrow t'} a_{t \rightarrow t'}$ is the transition probability from t to t' , broken down into the probability $g_{t \rightarrow t'}$ that tiling t' is generated as a possible successor to tiling t and the probability $a_{t \rightarrow t'}$ of actually accepting the succession.

Given $g_{t \rightarrow t'}$ and $g_{t' \rightarrow t}$, the acceptance probability of t' given t is defined as

$$a_{t \rightarrow t'} = \min \left\{ 1, \frac{e^{-\hat{S}(n'_1, n'_2)} g_{t' \rightarrow t}}{e^{-\hat{S}(n_1, n_2)} g_{t \rightarrow t'}} \right\}, \quad (25)$$

whence it follows that

$$\frac{a_{t \rightarrow t'}}{a_{t' \rightarrow t}} = \frac{e^{-\hat{S}(n'_1, n'_2)} g_{t' \rightarrow t}}{e^{-\hat{S}(n_1, n_2)} g_{t \rightarrow t'}}. \quad (26)$$

The definition in Eq. (25), therefore, leads directly to the condition in Eq. (24).

B. Successor generation

We assume $g_{t \rightarrow t'} > 0$ if and only if t' can be obtained from t either through the split of one tile (a domino or a tetramino) into two tiles (two squares or two dominoes, respectively) or through the merger of two tiles (two adjacent squares or two longitudinally adjacent dominoes) into one single tile (a domino or a tetramino, respectively). If $g_{t \rightarrow t'} > 0$ does indeed hold, then so does $g_{t' \rightarrow t} > 0$. It follows that the Markov chain in question is ergodic, that is, both aperiodic (since $\sum_{t'} g_{t \rightarrow t'} a_{t \rightarrow t'} < 1$, as there is always the possibility of rejection [35], so whenever transitioning from t it is possible to remain at t) and irreducible (i.e., any state can be reached from any other). Therefore, the chain has a unique stationary distribution, which as discussed in Section IV A is proportional to $e^{-\hat{S}}$.

Let n_s^t be the number of dominoes or tetraminoes in tiling t , and n_m^t the number of pairs of adjacent squares or pairs of longitudinally adjacent dominoes in t . The generation of t' from t starts with deciding which operation, the split of a domino into two squares or a tetramino into two dominoes (with probability p_s^t) or the merger of two adjacent squares or two longitudinally adjacent dominoes (with probability $p_m^t = 1 - p_s^t$), is to be applied. Probability p_s^t is given by

$$p_s^t = \frac{[n_s^t > 0]}{[n_s^t > 0] + [n_m^t > 0]}, \quad (27)$$

so p_s^t equals 0, 2^{-1} , or 1, since $n_s^t + n_m^t > 0$ always holds. Once the decision of whether to split or to merge has

been made, the tile to be split or the pair of tiles to be merged is chosen uniformly at random. We then have

$$g_{t \rightarrow t'} = \begin{cases} (n_s^t)^{-1} & \text{if } t' \in T_s^t \text{ and } n_m^t = 0, \\ (n_m^t)^{-1} & \text{if } t' \in T_m^t \text{ and } n_s^t = 0, \\ (2n_s^t)^{-1} & \text{if } t' \in T_s^t \text{ and } n_s^t n_m^t > 0, \\ (2n_m^t)^{-1} & \text{if } t' \in T_m^t \text{ and } n_s^t n_m^t > 0, \\ 0 & \text{if } t' \notin T_s^t \cup T_m^t. \end{cases} \quad (28)$$

In this equation, T_s^t comprises the n_s^t tilings obtainable from t via a split and T_m^t comprises the n_m^t tilings obtainable from t via a merger.

C. Implementation of the Wang-Landau method

Our implementation of the Wang-Landau method follows the steps outlined next, where hist_H and $\text{hist}_{\hat{S}}$ are histograms to record how many times each energy level is observed during the walker's traversal of the Markov chain and this level's entropy estimate, respectively. A parameter f is used to control the entropy estimates. It is set to 1 initially and is decreased to half its current value at each reset of hist_H . Termination occurs when $f < 10^{-10}$.

1. $t \leftarrow t_0$, where t_0 is a randomly chosen tiling;
Let h_t be the energy level of t ;
2. $\text{hist}_H(h) \leftarrow 0$ for every applicable energy level h ;
 $\text{hist}_{\hat{S}}(h) \leftarrow 0$ for every applicable energy level h ;
 $f \leftarrow 1$;
 $\text{hist}_H(h_t) \leftarrow 1$;
 $\text{hist}_{\hat{S}}(h_t) \leftarrow f$;
Go to Step 4;
3. $\text{hist}_H(h) \leftarrow 0$ for every applicable energy level h ;
4. Generate a tentative successor t' of t ;
With probability $a_{t \rightarrow t'}$, do $t \leftarrow t'$;
Let h_t be the energy level of t ;
If $\text{hist}_H(h_t) = 0$, go to Step 2;
 $\text{hist}_H(h_t) \leftarrow \text{hist}_H(h_t) + 1$;
 $\text{hist}_{\hat{S}}(h_t) \leftarrow \text{hist}_{\hat{S}}(h_t) + f$;
If hist_H is flat, do $f \leftarrow 2^{-1}f$ and go to Step 3;
If $f \geq 10^{-10}$, repeat Step 4;

The random walk starts at the randomly chosen tiling t_0 and is restarted whenever an energy level not yet encountered is found. Both initially and when a restart occurs, the two histograms hist_H and $\text{hist}_{\hat{S}}$ are reset in Step 2. Another opportunity for a reset, albeit a partial one, occurs when hist_H becomes flat and is then reset in Step 3. Flatness is detected in Step 4 whenever every energy level h encountered thus far has $\text{hist}_H(h)$ no lower than 95% of the histogram's average. Except for the resets in Steps 2 and 3, Step 4 keeps repeating until termination occurs. After this, for each energy level

h reached by the walker the entropy estimate is relativized to that of energy level $h^* = \arg \min_{h'} \text{hist}_{\hat{S}}(h')$, via $\text{hist}_{\hat{S}}(h) \leftarrow \text{hist}_{\hat{S}}(h) - \text{hist}_{\hat{S}}(h^*)$. In a run that reaches every energy level, h^* corresponds to the configuration $n_1 = mn, n_2 = 0$, that is, $h^* = 2mn - m - n$ and $k_{mn}(n_1, n_2) = 1$. In this case, the $\text{hist}_{\hat{S}}(h^*) = 0$ resulting from relativization is no longer an estimate but the exact value. Note that this holds automatically in the $m = 1$ case of Section III.

D. Handling degeneracy

As we normally do when handling the degenerate case, so too in the nondegenerate case we would like to associate an entropy estimate to each energy level directly. However, in general an energy level does not unequivocally determine a system configuration, so we opt instead to slightly alter the counting of squares and dominoes in a tiling. This is done by letting squares be counted in units of weight $1 + \epsilon_1$ and dominoes in units of weight $1 + \epsilon_2$. The values of ϵ_1, ϵ_2 must be sufficiently small to not affect the value of H in any meaningful way, while allowing any two distinct configurations that would otherwise have the same value of H to be told apart from each other by the now slightly different values of H .

In practice, this amounts to substituting $n_1(1 + \epsilon_1)$ for n_1 in Eqs. (3) and (4), and likewise $n_2(1 + \epsilon_2)$ for n_2 . From those two equations it follows that, to fulfill the purpose of identifying distinct configurations having the same value of H , we must have

$$3(n_1 - n'_1)(1 + \epsilon_1) \neq 2(n'_2 - n_2)(1 + \epsilon_2) \quad (29)$$

for all possible configurations n_1, n_2 and n'_1, n'_2 with $n_1 \neq n'_1$ or $n_2 \neq n'_2$. We use two randomly generated numbers of the order of 10^{-7} , viz., $\epsilon_1 = 7.72453 \times 10^{-7}$ and $\epsilon_2 = 1.47577 \times 10^{-7}$, which makes it impossible for the condition in Eq. (29) to be violated. Note that counting tiles in this slightly warped manner can be used directly in the nondegenerate case, by letting

$$\hat{S}_{\text{nd}}(n_1, n_2) = \text{hist}_{\hat{S}}(h), \quad (30)$$

where h is the energy level of configuration n_1, n_2 . It can also be used in the degenerate case, by coalescing together all energy levels having the same integral part. If $\mathcal{H}(\bar{h})$ is the set of all energy levels sharing the same integral part \bar{h} , then coalescing means letting

$$\hat{S}_{\text{d}}(\bar{h}) = \ln \sum_{h' \in \mathcal{H}(\bar{h})} e^{\text{hist}_{\hat{S}}(h')}. \quad (31)$$

E. The $m = 4$ and $m = n$ cases

In Sections IV F and IV G, we give results of the Wang-Landau method for $4 \times n$ and $n \times n$ boards. As previously, the possible values of H in Eq. (3), now considering only

their integral parts, range from a minimum that uses as many tetraminoes as possible, plus as few dominoes and squares as possible, to a maximum that uses squares exclusively.

For a $4 \times n$ board, this minimum occurs for configuration $n_1 = n_2 = 0, n_4 = n$ and equals

$$H_{\min}^{4 \times n} = 4(n-1). \quad (32)$$

The maximum occurs for configuration $n_1 = 4n, n_2 = n_4 = 0$ and equals

$$H_{\max}^{4 \times n} = 7n - 4. \quad (33)$$

As for an $n \times n$ board, first let $a = n \bmod 4$. The minimum integral part of an energy level can be seen to occur for configuration $n_1 = a^2 \bmod 2, n_2 = \lfloor a^2/2 \rfloor, n_4 = \lfloor n/4 \rfloor(n+a)$, which yields

$$H_{\min}^{n \times n} = 2(a^2 - 2\lfloor a^2/2 \rfloor) + 3\lfloor a^2/2 \rfloor + \quad (34)$$

$$5\lfloor n/4 \rfloor(n+a) - 2n \\ = 2a^2 - \lfloor a^2/2 \rfloor + 5\lfloor n/4 \rfloor(n+a) - 2n. \quad (35)$$

The maximum, in turn, occurs for configuration $n_1 = n^2, n_2 = n_4 = 0$, yielding

$$H_{\max}^{n \times n} = 2n(n-1). \quad (36)$$

Our computational experiments on $4 \times n$ and $n \times n$ boards were planned so that a board's number of cells would not exceed 256, as in Section III. Whenever the number of cells in use happens to be both a perfect square and a multiple of 4 (as is 256), a curious property, using n_{cells} to denote the number of cells, is that

$$\frac{3n_{\text{cells}}}{4} = H_{\max}^{1 \times n_{\text{cells}}} - H_{\min}^{1 \times n_{\text{cells}}} \quad (37)$$

$$= H_{\max}^{4 \times \frac{n_{\text{cells}}}{4}} - H_{\min}^{4 \times \frac{n_{\text{cells}}}{4}} \quad (38)$$

$$= H_{\max}^{\sqrt{n_{\text{cells}}} \times \sqrt{n_{\text{cells}}}} - H_{\min}^{\sqrt{n_{\text{cells}}} \times \sqrt{n_{\text{cells}}}}. \quad (39)$$

That is, the size of the energy spectrum is the same in all three cases. Also, and not surprisingly, the configurations for which the minimum and maximum value of H are obtained are the same in all three cases: $n_1 = n_2 = 0, n_4 = 64$ for the minimum, $n_1 = 256, n_2 = n_4 = 0$ for the maximum.

Fixing n_{cells} at 256 reveals further similarities. Not only are the two configurations of minimum and maximum energy the same in all three cases, but the set of 4225 configurations of the 1×256 case is the set of configurations of the 4×64 and 16×16 cases as well. To see that this is indeed the case, first consider that any configuration of either the 4×64 or the 16×16 case is also a configuration of the 1×256 case (simply arrange the tiles in the 1×256 board arbitrarily). Conversely, if at least one of m or n is a multiple of 4, then any configuration of the 1×256 case is also a configuration of both the 4×64 and 16×16 cases. This too is seen to be

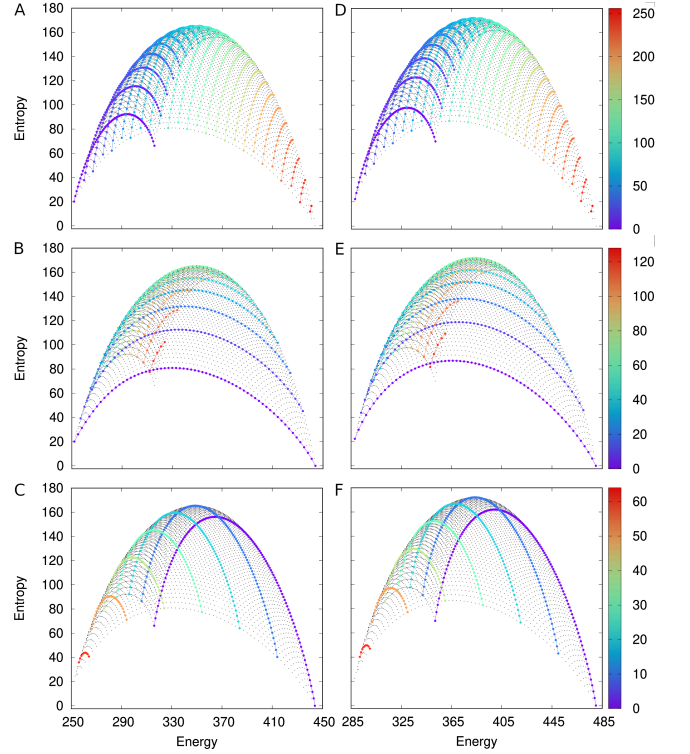


FIG. 6. As in Fig. 1, now for two cases of $m > 1$ with $n_{\text{cells}} = 256$, each configuration represented by its energy H and entropy \hat{S}_{nd} . (A–C) $m = 4, n = 64, H_{\min}^{4 \times 64} = 252, H_{\max}^{4 \times 64} = 444$; (D–F) $n = m = 16, H_{\min}^{16 \times 16} = 288, H_{\max}^{16 \times 16} = 480$. Color codes refer to multiple-of-10 values of n_1 (A, D), n_2 (B, E), or n_4 (C, F).

straightforward, for example assuming that m is a multiple of 4: first arrange the n_4 tetraminoes in columns of at most $m/4$ tiles each, then fill the remaining (partially filled or empty) columns with the n_2 dominoes and the n_1 squares.

These further similarities between the 1×256 , 4×64 , and 16×16 cases are important because they allow us to check the results output by the Wang-Landau method on the 4×64 and 16×16 boards against those we already validated analytically for the 1×256 board. The only differences we expect are significantly higher numbers of tilings, i.e., higher entropies and the corresponding adjustments in temperature. All else is expected to remain unaltered.

F. The nondegenerate case

Our results from the Wang-Landau method on the 4×64 and 16×16 boards, when degeneracy is disregarded so that phase separation can be observed, are summarized in the panels of Fig. 6. Each panel has exactly 4225 background dots, one for each configuration, indicating that the MCMC walker reached all of them. The likeness of the set of panels corresponding to the 4×64 board (A–

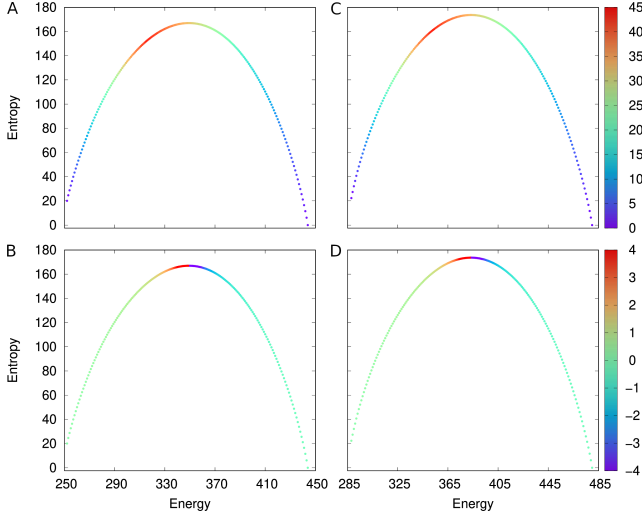


FIG. 7. As in Fig. 2, now showing entropy \hat{S}_d as a function of energy H for two cases of $m > 1$ with $n_{\text{cells}} = 256$. (A, B) $m = 4$, $n = 64$, $H_{\min}^{4 \times 64} = 252$, $H_{\max}^{4 \times 64} = 444$; (C, D) $m = n = 16$, $H_{\min}^{16 \times 16} = 288$, $H_{\max}^{16 \times 16} = 480$. Color codes refer to numbers of configurations (A, C) or to temperature \hat{T}_d (B, D).

C), or of those corresponding to the 16×16 board (D–F), to Fig. 1 cannot be missed. In fact, as expected, only the entropy values help distinguish one case from the other two. While for the 1×256 board we have $S_{\text{nd}} < 140$, for the 4×64 and 16×16 boards we have $\hat{S}_{\text{nd}} < 166$ and $\hat{S}_{\text{nd}} < 173$, respectively.

G. The degenerate case

When degeneracy is taken into account and all configurations for the same energy level are coalesced together, using the Wang-Landau method on the 4×64 and 16×16 boards yields the results shown in Fig. 7. This figure has two panels for the 4×64 board (A, B) and two for the 16×16 board (C, D). Two of the panels highlight the number of configurations contributing to each entropy value (A, C) and two others highlight the corresponding temperature (B, D). Temperature is now estimated from entropy differences, based on substituting the \hat{S}_d of Eq. (31) for S_d in Eq. (23). This results in

$$\hat{T}_d^{-1}(\bar{h}) \approx \frac{\hat{S}_d(\bar{h} + 1) - \hat{S}_d(\bar{h} - 1)}{2} \quad (40)$$

for the combined energy levels of integral part \bar{h} .

Once again, the resemblance of all four plots to the corresponding ones in Fig. 2 is hard to miss. Differences do exist, however, the clearest one relating to the maximum entropy levels in each case, as noted in Sec. IV F. The other difference has to do with the temperature estimates, which in all three cases are color-coded in the lower panels, but are nevertheless hard to discern visually.

H. Further remarks on computational tractability

We finalize Sec. IV by returning to the theme of computational tractability raised in Sec. III C in the context of the $m = 1$ special case, for which analytical treatment is possible. The concern in that case was centered on the total number of configurations. These had to be enumerated to exhaustion for use in the analyses, a process that we found out is severely limited as the number of cells in the board grows. The total number of tilings k_{1n} for each configuration, from which entropy is calculated, was in that case reason for no concern in terms of computational tractability, since the availability of a closed-form expression for k_{1n} was itself the one key factor enabling analytical treatment.

In the context of the $m > 1$ cases we have been handling in Sec. IV, the main concern related to computational tractability is the growth of the tiling space through which the MCMC walker navigates to estimate entropy. This space grows unimaginably quickly with both the total number of configurations for the different energy levels and especially the total number of tilings admitted by those configurations. A larger tiling space requires more steps for the walker to be able to roam sufficiently far and wide for convergence to occur. Figures 8 and 9 illustrate the growth trends of the two quantities.

Figure 8 is about the growth of the total number of configurations as n_{cells} grows. Panel A is for $4 \times \frac{n_{\text{cells}}}{4}$ boards, panel B for $\sqrt{n_{\text{cells}}} \times \sqrt{n_{\text{cells}}}$ boards. For each of these two cases we found the total number of configurations to asymptotically follow a power law similar to the quadratic one found for the $1 \times n_{\text{cells}}$ but still different from it. Figure 9, in turn, is about the growth of the total number of tilings as n_{cells} grows, with panels arranged analogously to Fig. 8. Exponentials in n_{cells} are still found, but now reaching significantly higher numbers. For $n_{\text{cells}} = 256$, a total number of tilings of the order of 10^{73} was found in the $4 \times \frac{n_{\text{cells}}}{4}$ case, of the order of 10^{76} in the $\sqrt{n_{\text{cells}}} \times \sqrt{n_{\text{cells}}}$ case. These are to be compared with the total number of tilings in the $1 \times n_{\text{cells}}$ case, which is of the order of 10^{63} .

Note, finally, that each total number of tilings plotted in Fig. 9 is estimated by summing up $\hat{K}(\bar{h})$ over the applicable values of \bar{h} , with

$$\hat{K}(\bar{h}) = \sum_{\bar{h}} e^{\hat{S}_d(\bar{h})}. \quad (41)$$

This quantity is the counterpart, for when analytical treatment is not possible, of the $K(h)$ defined in Eq. (19).

V. CONCLUSION

The scientific interest in tilings of the plane, and sometimes of higher-dimensional regions as well, has a history that spans several centuries. In the last six to seven decades, however, it gained new momentum motivated by

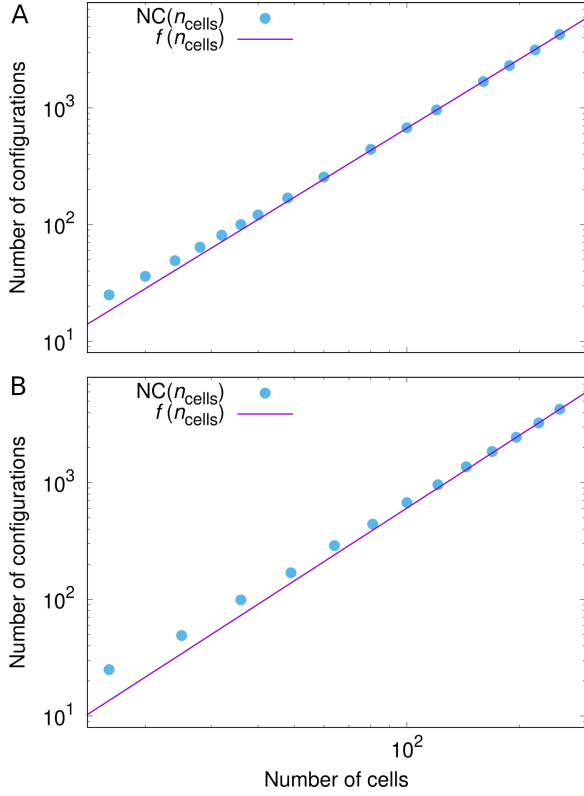


FIG. 8. As in Fig. 4, now as the function $\text{NC}(n_{\text{cells}})$ for two cases of $m > 1$ with $n_{\text{cells}} \leq 256$. (A) $m = 4$, $n = 4^{-1}n_{\text{cells}}$; (B) $m = n = \sqrt{n_{\text{cells}}}$. The power law that fits the points asymptotically is $f(n_{\text{cells}}) = 12.79^{-1}n_{\text{cells}}^{1.96648}$ (A) or $f(n_{\text{cells}}) = 23^{-1}n_{\text{cells}}^{2.07212}$ (B).

the realization in the early 20th century that some decision problems could be neither easy nor hard to solve, but simply undecidable. Though it soon turned out that undecidability was not an issue, interest did not wane. Instead, due to efforts by both mathematicians working on discrete systems and applied physicists in fields related to atomic- and molecular-scale phenomena, progress with important milestones was maintained. By and large, however, it seems fair to say that most key theoretical advancements, even those that inspired real-world applications, came from considering tilings of the whole, unbounded plane.

Studying tilings of bounded regions of the plane requires handling the combinatorics of finite discrete structures, a field in which exact closed-form expressions for counting quantities of interest are hard to come by. In this study, we considered rectangular regions of the plane and how to tile them with rectangular tiles. We concentrated on the tile-type set containing the square, the domino, and the straight tetramino. Simple though this system may seem, in the general case of an $m \times n$ board not even the number of configurations (how many squares, dominoes, tetraminoes) that are feasible can be counted exactly, not even indirectly via recurrence relations. Our approach has been to regard the system

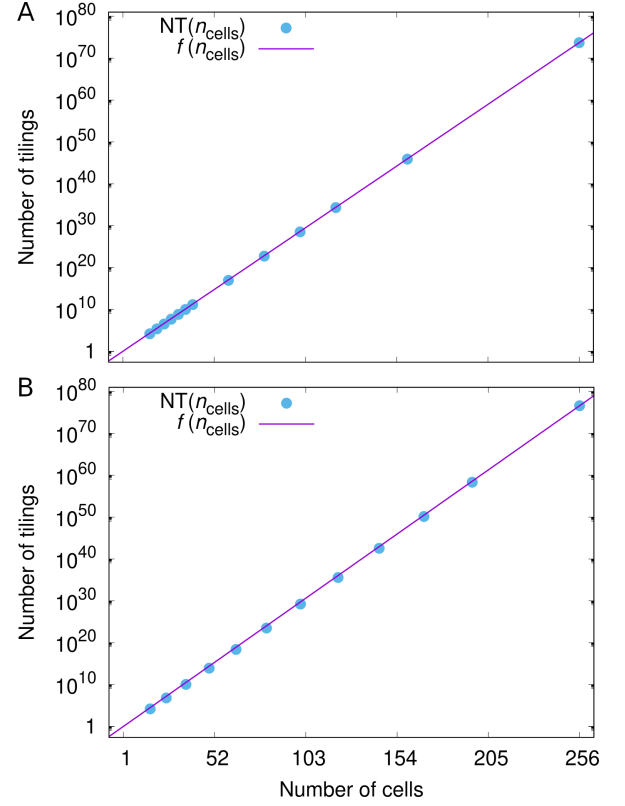


FIG. 9. As in Fig. 5, now as the function $\text{NT}(n_{\text{cells}}) = \sum_{\tilde{h}} \hat{K}(\tilde{h})$ for two cases of $m > 1$ with $n_{\text{cells}} \leq 256$. (A) $m = 4$, $n = 4^{-1}n_{\text{cells}}$; (B) $m = n = \sqrt{n_{\text{cells}}}$. The exponential that fits the points is $f(n_{\text{cells}}) = e^{0.665527(n_{\text{cells}}-1)}$ (A) or $f(n_{\text{cells}}) = e^{0.691678(n_{\text{cells}}-1)}$ (B).

from the standpoint of statistical physics and consider its configurations, states (tilings), energy, entropy, and temperature in such a way as to illuminate some of its inner workings. We followed two parallel tracks, one for the $m = 1$ case, the other for more general, $m > 1$ cases. Given our choice of a tile contact-based Hamiltonian, the $m = 1$ case is fully tractable analytically. The other track relied on the Wang-Landau method for state-density estimation in the $m > 1$ cases, and on the subsequent calculation of approximate entropies and temperatures. By alternately disregarding and taking into account the issue of energy-level degeneracy, we were able to demonstrate phase separation and thereby highlight how the system's configurations relate to one another, as well as to entropy and temperature.

A lot of room is left for methodological improvements. In particular, given the computationally intensive character of the Wang-Landau method, some of the techniques already developed for exploring the state space in parallel [36] should be considered. Additionally, our choice of Hamiltonian has been about the simplest imaginable. Considering the next level of sophistication, by adopting a Hamiltonian based on tile areas instead of simply perimeters, is bound to bring the entire approach closer

to some of the applications that might benefit from it. Some of these applications are in areas such as modeling biological tissues [37, 38] and their properties [39, 40], and developing bioinspired metamaterials [41].

ACKNOWLEDGMENTS

This work is part of the INCT-Física Nuclear e Aplicações project, No. 464898/2014-5. We acknowledge partial support from Conselho Nacional de Desenvolvimento Científico e Tecnológico (CNPq), Coor-

denação de Aperfeiçoamento de Pessoal de Nível Superior (CAPES), and a BBP grant from Fundação Carlos Chagas Filho de Amparo à Pesquisa do Estado do Rio de Janeiro (FAPERJ), as well as support from Agencia Nacional de Investigación e Innovación (ANII) and Programa de Desarrollo de las Ciencias Básicas (PEDECIBA). We thank Núcleo Avançado de Computação de Alto Desempenho (NACAD), Instituto Alberto Luiz Coimbra de Pós-Graduação e Pesquisa em Engenharia (COPPE), Universidade Federal do Rio de Janeiro (UFRJ), for the use of supercomputer Lobo Carneiro, where most of the calculations were carried out.

-
- [1] R. Berger, *The undecidability of the domino problem* (American Mathematical Society, Providence, RI, 1966).
 - [2] H. Wang, *Bell Syst. Tech. J.* **40**, 1 (1961).
 - [3] R. M. Robinson, *Invent. Math.* **12**, 177 (1971).
 - [4] R. Penrose, *Bull. Inst. Math. Appl.* **10**, 266–271 (1974).
 - [5] R. Penrose, *Eureka* **39**, 16 (1978).
 - [6] M. Gardner, *Penrose tiles to trapdoor ciphers* (The Mathematical Association of America, Washington, DC, 1997).
 - [7] D. Smith, J. S. Myers, C. S. Kaplan, and C. Goodman-Strauss, *arXiv:2303.10798* (2023).
 - [8] E. W. Weisstein, <https://mathworld.wolfram.com/Polykite.html>.
 - [9] D. Smith, J. S. Myers, C. S. Kaplan, and C. Goodman-Strauss, *arXiv:2305.17743* (2023).
 - [10] A. L. Mackay, *Physica A* **114**, 609–613 (1982).
 - [11] D. Shechtman, I. Blech, D. Gratias, and J. W. Cahn, *Phys. Rev. Lett.* **53**, 1951–1954 (1984).
 - [12] X. Zeng, B. Glettner, U. Baumeister, B. Chen, G. Ungar, F. Liu, and C. Tschierske, *Nat. Chem.* (2023).
 - [13] O. Stenull and T. C. Lubensky, *Phys. Rev. Lett.* **113**, 158301 (2014).
 - [14] F. Flicker, S. H. Simon, and S. A. Parameswaran, *Phys. Rev. X* **10**, 011005 (2020).
 - [15] H. Pan and J. Dshemuchadse, *ACS Nano* **17**, 7157 (2023).
 - [16] S. Wolfram, *Rev. Mod. Phys.* **55**, 601 (1983).
 - [17] P. W. K. Rothmund, N. Papadakis, and E. Winfree, *PLoS Biol.* **2**, e424 (2004).
 - [18] N. Kumar, Y.-S. Lan, C.-J. Chen, Y.-H. Lin, S.-T. Huang, H.-T. Jeng, and P.-J. Hsu, *Phys. Rev. Mater.* **6**, 066001 (2022).
 - [19] D. Woods, D. Doty, C. Myhrvold, J. Hui, F. Zhou, P. Yin, and E. Winfree, *Nature* **567**, 366 (2019).
 - [20] S. Dey, C. Fan, K. V. Gothelf, J. Li, C. Lin, L. Liu, N. Liu, M. A. D. Nijenhuis, B. Saccà, F. C. Simmel, H. Yan, and P. Zhan, *Nat. Rev. Methods Primers* **1**, 13 (2021).
 - [21] J. Xu, C. Chen, and X. Shi, *ACS Synth. Biol.* **11**, 2456 (2022).
 - [22] M. Kim, C. Lee, K. Jeon, J. Y. Lee, Y.-J. Kim, J. G. Lee, H. Kim, M. Cho, and D.-N. Kim, *Nature* **619**, 78 (2023).
 - [23] M. R. Garvie and J. Burkardt, *Contrib. Discret. Math.* **15**, 95 (2020).
 - [24] S. A. Cook, in *Proceedings of the Third Annual ACM Symposium on Theory of Computing* (Association for Computing Machinery, New York, NY, 1971) pp. 151–158.
 - [25] R. M. Karp, in *Complexity of Computer Computations*, edited by R. E. Miller and J. W. Thatcher (Plenum Press, New York, NY, 1972) pp. 85–103.
 - [26] F. Wang and D. P. Landau, *Phys. Rev. E* **64**, 056101 (2001).
 - [27] F. Wang and D. P. Landau, *Phys. Rev. Lett.* **86**, 2050 (2001).
 - [28] P. W. Kasteleyn, *Physica* **27**, 1209 (1961).
 - [29] H. N. V. Temperley and M. E. Fisher, *Philos. Mag.* **6**, 1061 (1961).
 - [30] M. Katz and C. Stenson, *J. Integer Seq.* **12**, 09.2.2 (2009).
 - [31] R. E. Belardinelli and V. D. Pereyra, *J. Chem. Phys.* **127**, 184105 (2007).
 - [32] G. Fort, B. Jourdain, E. Kuhn, T. Lelièvre, and G. Stoltz, *Math. Comput.* **84**, 2297–2327 (2015).
 - [33] N. Metropolis, A. W. Rosenbluth, M. N. Rosenbluth, A. H. Teller, and E. Teller, *J. Chem. Phys.* **21**, 1087–1092 (1953).
 - [34] W. K. Hastings, *Biometrika* **57**, 97 (1970).
 - [35] C. Andrieu, N. de Freitas, A. Doucet, and M. I. Jordan, *Mach. Learn.* **50**, 5 (2003).
 - [36] T. Vogel, Y. W. Li, T. Wüst, and D. P. Landau, *Phys. Rev. E* **90**, 023302 (2014).
 - [37] R. Farhadifar, J.-C. Röper, B. Aigouy, S. Eaton, and F. Jülicher, *Curr. Biol.* **17**, 2095–2104 (2007).
 - [38] D. L. Barton, S. Henkes, C. J. Weijer, and R. Sknepnek, *PLoS Comput. Biol.* **13**, e1005569 (2017).
 - [39] K. E. Cavanaugh, M. F. Staddon, E. Munro, S. Banerjee, and M. L. Gardel, *Dev. Cell* **52**, 152 (2020).
 - [40] J.-A. Park, J. H. Kim, D. Bi, J. A. Mitchel, N. T. Qazvini, K. Tantisira, C. Y. Park, M. McGill, S.-H. Kim, B. Gweon, J. Notbohm, R. Steward Jr., S. Burger, S. H. Randell, A. T. Kho, D. T. Tambe, C. Hardin, S. A. Shore, E. Israel, D. A. Weitz, D. J. Tschumperlin, E. P. Henske, S. T. Weiss, M. L. Manning, J. P. Butler, J. M. Drazenl, and J. J. Fredberg, *Nat. Mater.* **14**, 1040 (2015).
 - [41] A. Parker, *Phys. Today* **74**, 30 (2021).